

# Morphology and Surface Brightness Evolution of $z \sim 1.1$ Radio Galaxies

Nathan Roche, Stephen Eales

Department of Physics and Astronomy, University of Cardiff,  
P.O. Box 918, Cardiff CF2 3YB, Wales.

Steve Rawlings

Department of Astrophysics, University of Oxford,  
Nuclear and Astrophysics Laboratory, Keble Road, Oxford OX1 3RH, England.

## Abstract

We use  $K'$ -band ( $2.1 \mu\text{m}$ ) imaging to investigate the angular size and morphology of 10 6C radio galaxies, at redshifts  $1 \leq z \leq 1.4$ . Two appear to be undergoing mergers, another contains two intensity peaks aligned with the radio jets, while the other seven appear consistent with being normal ellipticals in the  $K$ -band.

Intrinsic half-light radii are estimated from the areas of each radio galaxy image above a series of thresholds. The 6C galaxy radii are found to be significantly smaller than those of the more radioluminous 3CR galaxies at similar redshifts. This would indicate that the higher mean  $K$ -band luminosity of the 3CR galaxies results from a difference in the size of the host galaxies, and not solely from a difference in the power of the active nuclei.

The size-luminosity relation of the  $z \sim 1.1$  6C galaxies indicates a 1.0–1.8 mag enhancement of the rest-frame  $R$ -band surface brightness relative to either local ellipticals of the same size or FRII radio galaxies at  $z < 0.2$ . The 3CR galaxies at  $z \sim 1.1$  show a comparable enhancement in surface brightness. The mean radius of the 6C galaxies suggests that they evolve into ellipticals of  $L \sim L^*$  luminosity, and is consistent with their low redshift counterparts being relatively small FRII galaxies, a factor  $\sim 25$  lower in radio luminosity, or small FRI galaxies a factor of  $\sim 1000$  lower in radio luminosity. Hence the 6C radio galaxies may undergo at least as much optical and radio evolution as the 3CR galaxies.

## 1. Introduction

Powerful radio galaxies at  $z < 0.5$  appear similar in morphology and profile to normal giant ellipticals (Lilly, MacLean and Longair 1983), with luminosities in the range from  $L^*$  to  $\sim 2$  mag above  $L^*$  and no obvious correlation between radio and optical luminosity (Laing, Riley and Longair 1983; Owen and Laing 1989; Owen and White 1991). The relative uniformity of the optical properties of radio galaxies, combined with the ease of detection at higher redshifts, means that they provide a useful probe of galaxy evolution. Lilly and Longair (1984) measured  $K$ -band ( $2.2 \mu\text{m}$ ) magnitudes for 3CR radio galaxies over a very wide range of redshifts (the 3CR catalog is a flux limited sample containing the radio galaxies with apparent flux exceeding 10 Jy at 178 MHz). The  $K$ - $z$  relation of these galaxies, which showed little

scatter out to  $z \sim 2$ , indicated an evolutionary brightening with redshift, consistent with a high formation redshift ( $z \sim 5$ ) followed by passive stellar evolution.

The radio luminosities of the most powerful radio galaxies also evolve. Laing, Riley and Longair (1983), using a  $V/V_{max}$  test, showed that their decrease in luminosity with time was comparable to the evolution of quasars. Padovani and Urry (1992) studied the radio evolution of the 3CR catalog in more detail, deriving a radio luminosity function and obtaining a best fit for an exponential  $L_{rad}$  evolution with timescale  $\tau = 0.17_{-0.02}^{+0.03} H_0^{-1}$  i.e.  $\tau = 3.3_{-0.4}^{+0.6}$  Gyr. It must be noted that this exponential decrease describes the evolution of the radio luminosity function, rather than that of individual radio galaxies. The galaxies might, for example, undergo short bursts of radio emission, separated by much longer periods of radio quiescence, with subsequent bursts decreasing with time in their peak radio intensity.

Higher redshift radio galaxies differ in appearance from normal ellipticals, especially at shorter wavelengths. Rigler et al. (1992) studied 13 3CR galaxies at  $0.8 < z < 1.3$  and found that they could be decomposed into ‘active’ and ‘passive’ components. The ‘active’ components were elongated, blue (approximately  $f_\nu \propto \nu^0$ ), and aligned with the radio axis. Best et al. (1996), using WFPC2 imaging, found that in radio galaxies with a relatively small separation between the radio lobes, the blue components consisted of strings of several bright knots, whereas in radio galaxies with radio lobes separated by more than  $\sim 200$  kpc, the blue components were much more compact. This suggested an evolutionary sequence in which the elongated optical components were formed as the outward passage of the radio jets triggers large-scale star-formation, and later fall back towards the galaxy centres. However, the aligned components of at least some  $z \sim 1$  radio galaxies show some polarization (Tadhunter et al. 1992; Leyshon and Eales 1997), suggesting that dust-reflected light from the active nucleus is also important.

The aligned components are less prominent at longer wavelengths, typically contributing only  $\sim 10\%$  of the total flux at  $\lambda_{rest} \simeq 1\mu\text{m}$  (i.e. the observed  $K$ -band), but many of the  $z \sim 1$  3CR galaxies still show some alignment between their radio axes and  $K$ -band isophotes (Dunlop and Peacock 1993; Ridgway and Stockton 1997). Most of the red light is produced by the ‘passive’ components, which are redder, diffuse and symmetric, apparently unaligned with the radio axis, and appear to be underlying giant ellipticals.

In the infra-red  $H$ -band ( $1.65\mu\text{m}$ ), Rigler and Lilly (1994) found the profile of the  $z = 1.18$  radio galaxy 3C65 to be well-fitted with a pure bulge ( $r^{\frac{1}{4}}$ ) profile of effective radius  $r_e = 1.77 \pm 0.18$  arcsec. Best et al. (1997), observing in the  $K$ -band and with the HST WFPC2, confirmed  $r_e = 1.7$  arcsec for 3C65, and found all 21 of a sample of  $z \sim 1$  3CR galaxies to be well-fitted by bulge models with  $0.7 < r_e < 3.9$  arcsec. The size-luminosity relation of these galaxies was consistent with that of local ellipticals with the  $\sim 1^m$  of brightening expected from passive evolution. Only two of the 21 galaxies contained substantial ( $> 10\%$  of total flux) nuclear point-sources components, although several showed some evidence of an excess of surface brightness above a bulge-model profile at large radii ( $r > 35$  kpc), like that in cD galaxies, which might be evidence for a rich cluster environment.

In this paper we investigate the  $K$ -band morphology and radii of 10 galaxies at similar redshifts but with more moderate radio luminosities, selected from the 6C survey which has a flux limit about six times fainter than 3CR. There are some unsolved problems concerning the differences between the 3CR and 6C galaxies. Firstly, 6C radio galaxies at  $0.6 < z < 1.8$  were found to be on average 0.7 mag less luminous in the observed  $K$ -band than 3CR galaxies at the same redshifts (Eales and Rawlings 1996; Eales et al. 1997), but it was unclear whether this was due solely to a greater near-IR flux from the 3CR nuclei, or to a greater mass of stars in the 3CR galaxies. We shall investigate whether the differences in the radio and optical luminosities of 3CR and 6C galaxies at  $z \sim 1$  are related to any differences in the old stellar component visible in the  $K$ -band. Secondly, as the 3CR and 6C galaxies at lower redshifts are similar in mean  $K$ -band luminosity, the  $K$ - $z$  relations of the 3CR and 6C catalogs are different in slope, with the latter consistent with no evolution. Hence if high redshift 6C galaxies evolve into the low redshift 6C galaxies, they undergo surprisingly little change in  $K$ -band luminosity, but it is also possible that their low redshift counterparts are galaxies of lower  $K$  and radio luminosity. By determining a size-luminosity relation for the 6C galaxies and comparing with both  $z \sim 1$  3CR galaxies and low-redshift radio galaxies (from Owen and Laing 1989), we may compare the surface brightness evolution of the two catalogs and determine whether the 6C galaxies are truly non-evolving.

We assume  $H_0 = 50 \text{ km s}^{-1} \text{ Mpc}^{-1}$  and  $q_0 = 0.05$  throughout. Section 2 describes the observational data, Section 3 its analysis and photometry. In Section 4 we describe the estimation of the size and morphological type of the galaxies, and in Section 5 discuss the appearance of each individual 6C galaxy. In Section 6 we present the size-luminosity relation and compare with 3CR galaxies at similar redshifts and local radio galaxies, and in Section 7 discuss the implications for radio galaxy evolution. Section 8

summarizes the main conclusions.

## 2. Observational Data

The observational dataset of this paper consists of 10 images, each centred on a 6C radio galaxy with a known spectroscopic redshift in the  $1.0 \leq z \leq 1.4$  range ( $z_{mean} = 1.11$ ). This data was previously used by Eales et al. (1997) in a study of the  $K$ -band luminosity evolution of radio galaxies. The 6C galaxies considered here have 151 MHz fluxes of 2.2–4.4 Jy, corresponding at these redshifts to  $L(151\text{MHz}) \sim 10^{28.6} \text{ W Hz}^{-1}$ . Allington-Smith (1982) and Eales (1985) give more information on the radio source properties, Eales et al. (1997) and references therein detail the identification of the optical counterparts, and Rawlings et al. (1997) describe the spectroscopic observations. For comparison we include in our dataset an image of a radio-loud QSO, 5C6.8, which lies in the same redshift range as the other objects. Table 1 lists the radio galaxy co-ordinates and redshifts for all 11 images.

These fields were observed over the period 18–20 January 1995 using the Redeye camera on the Canada-France Hawaii Telescope (CFHT). Redeye is a  $256 \times 256$  HgCaTe mosaic with a pixelsize of 0.50 arcsec, covering approximately  $2 \times 2$  arcmin. Each field was imaged nine times, with the camera being offset by 8 arcsec between exposures in a  $3 \times 3$  grid. The total exposure times varied from 26 to 47 minutes per field. The observations were made in the the  $K'$  band, centred on a wavelength of  $2.1 \mu\text{m}$  where there is some reduction of sky background compared to that in the standard  $2.2 \mu\text{m}$   $K$ -band (Wainscoat and Cowie 1992). All 11 images had good seeing, estimated as  $FWHM \simeq 0.9\text{--}1.2$  arcsec.

## 3. Data Analysis and Galaxy Detection

After initial image processing using the IRAF package (see Eales et al. 1997), the Starlink PISA (Position, Intensity and Shape Analysis) package, developed by M. Irwin, P. Draper and N. Eaton, was used to detect and catalog the objects on each field. Object were detected on the basis that they exceed an intensity threshold of  $1.5\sigma$  above the background noise ( $\sigma$  being separately determined by PISA for each of the frames) in at least 6 connected pixels. Fluxes were estimated using the ‘total magnitudes’ option within PISA, which counts photons above the sky background level in elliptical apertures about the centroid of each detection, with the aperture size and shape being fitted by a curve-of-growth analysis to the intensity profile of each object.

Observations of  $K$ -band standard stars provided a photometric zero-point for the Redeye data of  $K = 21.28$  for 1 count  $\text{sec}^{-1}$ . However, due to the offset between the  $K$  and  $K'$  passbands, this zero point will be exact only for objects with the same  $K' - K$  as the standard stars. Radio galaxies with elliptical-like colours will at  $1 \leq z \leq 1.4$  be redder than the calibration stars by an estimated  $\Delta(K' - K) \simeq 0.13$  mag (see Eales et al. 1997), so to correct for this we add  $\Delta(K) = -0.13$  mag to the magnitudes, adopting a zero-point of  $K = 21.15$  for 1 count  $\text{sec}^{-1}$ .

PISA also produces a list of 8 areas for each detected object. The first area is simply the number of pixels where the intensity equals or exceeds the chosen detection threshold, while sizes 2–8 are the areas above higher thresholds of  $I_{thr} + 2^{j+2}$  counts, where  $I_{thr}$  is the threshold and  $j$  an integer from 2 to 8. For these images,  $I_{thr} \sim 50$  counts so the 8th threshold would be  $\sim 1074$  counts and  $\sim 7.5$  mag above the detection threshold.

We are only concerned here with the radio galaxies on each image; the properties (e.g. clustering) of the other galaxies detected will be discussed in a separate paper. Figures 1 and 2 show greyscale images and contour plots of  $15 \times 15$  arcsec areas centred on each radio galaxy. Table 1 lists the  $K$ -band total magnitudes of the radio galaxies, as measured from this data (with errors estimated from the best-fitting models described in Section 4 below). These are consistent with the magnitudes of Eales et al. (1997). Table 1 also lists the detection thresholds of the 11 images in terms of  $K$  mag  $\text{arcsec}^{-2}$ . Two of the radio galaxies were detected by PISA as double objects on these images, 6C011+36 with components of apparent separations 1.7 arcsec and 6C1256+36 with components of separation 2.5 arcsec. These pairs are still connected at the detection threshold so are only split when PISA is run with the ‘deblend’ option. In this analysis we have used PISA without deblending, so these radiogalaxies are classed as single objects, and the derived magnitudes and areas will be those of both components together.

## 4. Estimating Galaxy Sizes and Profiles

### 4.1 Method

Most of the radio galaxies appear extended on these images. To estimate their intrinsic angular sizes and distinguish between disk and bulge profiles, we compare their areas above 8 thresholds as given by PISA with those measured for simulated galaxy profiles. We consider three types of source profile

(i) A point source.

(ii) An exponential disk, with surface brightness  $\mu \propto \exp(-r/r_{exp})$ . We consider exponential scale-lengths in the range  $0.07 \leq r_{exp} \leq 1.00$  arcsec. The half-light radius  $r_{hl} = 1.68r_{exp}$ .

(iii) A bulge (elliptical galaxy) profile, with surface brightness  $\mu \propto \exp -7.67(r/r_e)^{0.25}$ . We consider effective radii ( $r_e$ ) in the range  $0.07 \leq r_e \leq 3.00$  arcsec. For this profile  $r_{hl} = r_e$ .

Each model profile was generated on a 0.1 arcsec pixel grid, and then rebinned into 0.5 arcsec pixels. The model profiles were arranged in a grid pattern on a ‘simulation image’, with each model profile represented 12 times with slightly different positional offsets relative to the 0.5 arcsec pixel grid. The seeing profile was estimated for each image by fitting (using a PISA routine) a combined Gaussian-exponential-Lorentzian to a few objects identified as stars (of similar apparent magnitude to the radio galaxies). The simulation image was then convolved with the model stellar profile and normalized so that the model profiles had the same total intensity as measured for the radio galaxy. Gaussian noise was then added to the simulation image, with  $\sigma$  equal to the sky noise as measured on the real data.

The simulation image was then analysed using PISA, with the same detection threshold as used for the radio galaxy data. For each model profile, this gave 12 sets of areas above the 8 thresholds, with some scatter between the 12 due to the modelled sky noise and the positional offsets between the models. These 12 sets of areas were averaged to give a set of 8 PISA areas corresponding to each model profile, with error bars calculated from the scatter. For each radio galaxy we then compared the observed set of 8 areas with those measured for each of the models, using a  $\chi^2$  test with the simulation errors.

Table 2 shows the results of this comparison for each object, with  $\chi^2$  for the point-source models, the exponential scalelength ( $r_{exp}$ ) and  $\chi^2$  of the disk-profile model which best fits the observed set of 8 areas, i.e. which gives the smallest  $\chi^2$ , and the effective radius ( $r_e$ ) and  $\chi^2$  of the best-fitting bulge model.

For a  $\chi^2$  test with 7 degrees of freedom, we would expect a ‘perfect’ model to on average give  $\chi^2 \simeq 6.4$ , and would estimate  $\pm 1\sigma$  errors on  $r_{exp}$  and  $r_e$  as the change in the model radius above or below the best-fitting model which increases  $\chi^2$  by 8.16 above its minimum value. However, in this analysis the 8 areas given by PISA are not entirely independent; a large noise fluctuation could change a pixel’s value by more than one threshold interval, thus altering more than one of the areas. To take this into account, we also  $\chi^2$ -test the observed areas above thresholds against each of the 12 representations of the best-fitting model in our simulation image, obtaining 12 values of  $\chi^2$ . The scatter in these 12 values of  $\chi^2$  gives the  $\pm 1\sigma$  errors (listed in Table 2) produced by noise on the best-fit model’s  $\chi^2$ . The errors on the best-fit  $r_e$  and  $r_{exp}$  can be estimated as the change in these radii which increases  $\chi^2$  above that of the best-fit model by these  $1\sigma$  noise errors. However, the true errors on the size estimates may be somewhat larger due to the approximate modelling of the point-spread function and to asymmetry and substructure in the real radio galaxies.

## 4.2 Results

Firstly, the point-source models are generally a poor fit, giving a large  $\chi^2$ . Using the estimated noise errors on  $\chi^2$ , we can quantify the rejection of a point-source profile as  $\sim 2\sigma$  for 6C1017+37, but  $\sim 6$ – $20\sigma$  for the other 9 radio galaxies. Even for the QSO, a pure point-source is rejected by  $6.7\sigma$ . For all objects except 6C1256+36 and the QSO, there is a disk model and/or a bulge model with a  $\chi^2$  sufficiently low to indicate consistency within  $2\sigma$ . In some cases,  $\chi^2$  is very similar for the best-fit disk and bulge models, for other galaxies one model may be favoured by as much as several  $\sigma$ .

Figure 3 shows histograms of the area of each radiogalaxy above the 8 thresholds, together with the areas derived from the point-source model and the best-fitting disk and bulge models. To compare the models and data more directly, we also show radial intensity profiles. Figure 4 shows the mean  $K$ -band intensity in  $\Delta(r) = 0.5$  arcsec annuli about the centroid of each radio galaxy, together with the point-source profile and the best-fitting disk and bulge models.

Table 2 lists the apparent surface brightness (SB) of each galaxy within the central 0.5 arcsec. This will correspond only approximately to the intrinsic properties of the galaxies, but does show some differences between them. The mean apparent central SB is  $19.07 \pm 0.13$   $K$  mag arcsec $^{-2}$  for the 10 6C radio galaxies, but the QSO is significantly higher in central SB and the galaxies 6C1017+37 and 6C1129+37 are particularly low. The morphologies of the individual galaxies are described below.

## 5. Morphology of Individual Radio Galaxies

1. 6C0822+39 appears symmetric with a profile well-fitted by the bulge model, which is strongly ( $\sim 4\sigma$ ) favoured over a disk model. This galaxy appears in the  $K$ -band to be a normal elliptical.

2. 6C0943+39 is small symmetric object, consistent with either disk or bulge at the  $1\sigma$  level. On the basis of this data, it could be another normal elliptical.

3. 6C1011+36 is small and asymmetric with a much fainter secondary nucleus 1.7 arcsec from the main nucleus but clearly within the outer envelope, suggesting that it is currently merging with a much smaller galaxy. It may also be interacting with two close companions, which produce the peak in the profile at  $r \sim 4$  arcsec. Neither a disk or a bulge profile is strongly favoured.

4. 6C1017+37 is another small symmetric object, apparently the smallest of these galaxies. It is consistent with either disk or bulge models at the  $1\sigma$  level, and the only galaxy consistent at the  $< 3\sigma$  level with being a point-source. The low central SB is presumably due to the object being faint and unresolved, rather than being an intrinsically low SB galaxy. There is no excess above the fitted models at either small or large radii, so this object could simply be a small elliptical.

5. 6C1123+34 is round and symmetric, with a profile consistent with both the disk and bulge models. There is another galaxy about 5.5 arcsec away but no obvious indication that the two are interacting. This could be a normal elliptical.

6. 6C1129+37 is extended and asymmetric with two intensity peaks of similar luminosity. These lie well within the same envelope, so that PISA detects 6C1129+37 as a single galaxy even with the deblend option. The outer regions appear disturbed with some evidence of trails, especially to the north. This is the only galaxy in this sample for which the profile significantly ( $\sim 4\sigma$ ) favours an exponential model over a bulge model. It also has a low central SB (0.49 mag less than the sample mean) which, as the galaxy is clearly resolved, would imply that the intrinsic central SB is lower than that of the other radio galaxies. A recent red-band WFPC2 image of this galaxy, to be described in detail by Best et al. (in preparation), also showed that

(i) the two peaks seen on the  $K$  image (centroids separated by 1.9 arcsec) lie within elongated structures with tails pointing *inwards* to the galaxy centre, suggesting that they are ‘hotspots’ associated with the outward passage of the radio jets rather than the two components of a merger. Close to the centre the jets appear to be aligned with the 137 degree position angle of the two peaks of radio emission (Allington-Smith 1982; Eales et al. 1997), although the two radio lobes lie much further out, being separated by 14 arcsec. Further out from the centre, the  $R$ -band jets curve slightly toward a W–E axis, causing the  $K$ -band peaks to be slightly misaligned from the radio axis.

(ii) The faint extension to the north is a small spiral galaxy of high  $R$ -band ( $\lambda_{\text{rest}} \simeq 3000\text{\AA}$ ) SB, which appears to be interacting with the larger radio galaxy. Allington-Smith et al. (1982) had previously found 6C1129+37 to be double on a ground-based  $R$ -band CCD image, with the two components separated north-south so presumably corresponding to the radio galaxy and this companion rather than the two radio jet hotspots.

(iii) No central point source is visible at  $\lambda_{\text{rest}} \simeq 3000\text{\AA}$ .

7. 6C1204+35 appears symmetric, slightly favouring ( $\sim 1\sigma$  level) a bulge over a disk profile. There is no excess above the fitted bulge model at large radii. This galaxy seems consistent with being a normal elliptical.

8. 6C1217+36 is extended with a bulge profile favoured over an exponential disk by  $\sim 2\sigma$ . The outer regions look slightly asymmetric, with some isophotal twist apparent on the contour plot. The radial profile is very close to the bulge model except for a small excess at  $r \sim 5$  arcsec due to a much smaller companion galaxy. This could, for example, be a normal elliptical just slightly perturbed by a near-miss encounter, resulting in a slight asymmetry.

9. 6C1256+36 is extended and double with a less luminous secondary nucleus, 2.5 arcsec from the main nucleus. The outer regions are asymmetric and much more extended than in the other double galaxy (6C1011+36), with the second nucleus lying within what appears to be an inclined disk. The galaxy may also be interacting with its much smaller nearby companion (there is a hint of a bridge between the two). The galaxy is not fitted well by either a disk or bulge model, having too much area at the lowest thresholds. However, the radial profile looks closer to the bulge model at  $r < 2$  arcsec, and the central SB

is typical of this sample (in contrast to 6C1129+37), suggesting that the primary galaxy is an elliptical. This is consistent with the visual impression of an elliptical merging with a large, lower SB disk galaxy.

10. 6C1257+36 is closer to a bulge profile than a disk, although only by  $\sim 1\sigma$ . The profile is well-fitted by the bulge model except for an excess at  $r \sim 4$  arcsec, due to a small companion galaxy. This galaxy could be another normal elliptical.

11. The QSO 5C6.8 contains a very bright central nucleus, giving a central SB higher than that of any of the 10 radio galaxies, and a very small  $r_{hl}$ . However, the object is not a pure point source. The  $K$ -band image also shows the extended, lower surface brightness host galaxy, which appears disturbed, suggesting a recent merger or interaction. The profile is close to the fitted models at  $r < 3$  arcsec but shows a significant excess at  $r \simeq 4$  arcsec, where it is more extended and resembles the profiles of the radio galaxies. Consequently, neither the disk or bulge models are a good fit, and a pure point-source model is also rejected. Two-component models and higher resolution data would be needed to investigate two-component systems of this type, by separately estimating a point-source contribution and an  $r_{hl}$  for the underlying galaxy (see Best et al. 1997).

Despite the long wavelength of observation, these galaxies show a significant morphological diversity as well as a wide range of half-light radius. Two galaxies, 6C1011+36 and 6C1256+36 appear to be merging doubles. The 6C1129+37 galaxy is especially unusual - it is interacting and has luminous features associated with the radio emission visible on the  $K$ -band image. We refer to this for now as a ‘radio jet object’.

Dunlop and Peacock (1993) and Ridgway and Stockton (1997) found that many  $z \sim 1$  3CR galaxies do show an alignment between their  $K$ -band isophotes and radio axes, although no alignment was seen for Parkes radio galaxies an order of magnitude less radioluminous. Our 6C sample is intermediate in radio luminosity, so might be expected to contain at least one galaxy with visible  $K$ -band/radio alignment. The 6C1129+37 galaxy appears to be the only galaxy of these 10 with resolved aligned features, but it may also be significant that 6C0943+39, 6C1017+35 and 6C1204+35 show a close alignment (within  $\sim 10$  degrees) of their  $K$ -band position angles and radio axes (Eales et al. 1997).

The 6C1129+37 galaxy is also the only object in this sample with a  $K$ -band profile which appears to significantly favour an exponential over a bulge model. Further observations may be needed to determine whether it is truly a disk galaxy or an elliptical with a profile distorted by the interaction and radio hotspots, but the low central SB compared to the other large double galaxy (6C1256+36), might favour a later Hubble type.

The other seven galaxies appear at least consistent with the elliptical morphology seen for most radio galaxies, so will be referred to for now as ‘bulge/generic’ galaxies. We now consider the relation between angular size, luminosity and morphology for these and other radio galaxies.

## 6. Size vs. Absolute Magnitude Relation

We estimate the absolute magnitudes of the radio galaxies in the rest-frame Cousins  $R$ -band ( $\lambda_{\text{cent}} \simeq 6560\text{\AA}$ ), by subtracting the distance modulus from each observed  $K$  magnitude (Table 1), and adding a modelled correction to convert from the observer-frame  $K$ -band to the rest-frame  $R$ -band.

Roche et al. (1997) describe a model for the evolution of E/S0 galaxies, in which star-formation begins at a high redshift, 16.5 Gyr ago, and decreases rapidly with an exponential timescale  $\tau_{\text{SFR}} = 0.5$  Gyr. As almost all star-formation occurs at  $z > 3$ , the evolution is passive at the redshifts we are concerned with here. The star-formation history is converted into an evolving spectral energy distribution using the stellar evolution models of Charlot and Bruzual (1993), and assuming a Salpeter IMF. Figure 5 shows the  $R_{\text{rest}} - K_{\text{obs}}$  correction, as a function of redshift, derived from this model’s evolving spectral energy distribution, and also shows  $R_{\text{rest}} - K_{\text{obs}}$  from much a bluer model in which star-formation begins at the same epoch but continues at a constant rate.

At  $z = 1.1$ , the constant SFR model predicts much bluer observer-frame colours than the E/S0 model,  $R - K = 3.5$  compared to  $R - K = 5.5$ , but the  $R_{\text{rest}} - K_{\text{obs}}$  correction differs by only 0.21 mag. At  $z \sim 1$ , many radio galaxies have  $R - K$  colours close to a passively evolving model, which essentially defines the red envelope of their colour-redshift distribution, but some of the more radioluminous (i.e. 3CR) galaxies are as much as  $\sim 2$  mag bluer and would be closer to the constant SFR model (Lilly and Longair 1984; Dunlop and Peacock 1993). Assuming an E/S0 model should therefore give a conservative estimate of  $M_R$ , accurate for the redder galaxies but an underestimate by as much as 0.21 mag for any objects which are as blue as the bluest 3CR galaxies.

Table 3 gives our estimates of  $M_R$ . All of these 6C galaxies are more luminous than the zero-redshift  $L^*$  ( $M_R \simeq -22.57$  for ellipticals), with a mean  $M_R$  for the radio galaxies (excluding the QSO) of  $-24.25 \pm 0.18$ . To investigate the  $M_R - r_{hl}$  relation, we adopt the disk model size estimate,  $r_{hl} = 1.68 r_{exp}$  for all objects with a smaller minimum  $\chi^2$  for the disk model (6C1011+36, 6C1017+37, 6C1129+37, 6C1256+36) and the bulge model estimate  $r_{hl} = r_e$  for the others. Note that adopting instead the bulge-model  $r_{hl}$  for the four objects with a lower  $\chi^2$  for the disk-model would increase the errors on their  $r_{hl}$  estimates, but would not significantly change their best-fit  $r_{hl}$ . If disk galaxy is observed at an inclined angle its apparent area will be reduced. To estimate the intrinsic size of inclined galaxies we would obviously use  $r_{hl}$  on the major axis rather than the smaller  $r_{hl}$  derived from the apparent area. The observed area relative to that seen if the galaxy was seen face-on will be approximately  $(1 - e)$ , where  $e$  is the image ellipticity as measured by PISA. We therefore correct the  $r_{hl}$  estimates for inclination by multiplying by  $(1 - e)^{-0.5}$ . Table 3 gives the ellipticities and corrected  $r_{hl}$  estimates, again with  $\pm 1\sigma$  errors, both in arcsec and in kiloparsecs for the assumed cosmology. The unweighted mean of the  $r_{hl}$  estimates for the radio galaxies (excluding the QSO) is  $6.1 \pm 1.3$  kpc.

Figure 6 shows  $r_{hl}$  against  $M_R$  for these galaxies, with symbols indicating morphological types, together with the 21 3CR galaxies from Best et al. (1997), with the fitted bulge-model radii converted to kpc for our assumed cosmology. These 3CR galaxies cover a wide redshift range of  $0.47 < z < 1.27$ , with  $z_{mean} = 0.89$  compared to our sample's  $z_{mean} = 1.11$ , so were divided into two subsamples, the 9 galaxies at  $z > 0.93$ , with a mean redshift ( $z_{mean} = 1.10$ ) almost identical to our 6C sample, and the 12 at  $z < 0.93$ , with  $z_{mean} = 0.73$ . The absolute magnitudes of the 3CR galaxies were estimated using the  $K$ -band aperture magnitudes of Lilly and Longair (1984), extrapolated to total magnitudes assuming bulge profiles with  $r_e$  from Best et al. (1997), and adopting the same E/S0 model  $R_{rest} - K_{obs}$  correction as used for the 6C galaxies.

The 3CR galaxies are on average more luminous (mean  $M_R = -24.88 \pm 0.15$ ) and much larger (mean  $r_{hl} = 17.9 \pm 1.5$  kpc) than the 6C galaxies. The 3CR galaxies at  $0.93 < z < 1.27$  are more luminous (mean  $M_R = -25.30 \pm 0.16$ ) than those at  $0.47 < z < 0.93$  (mean  $M_R = -24.56 \pm 0.19$ , but not significantly different in size (mean  $r_{hl} = 17.5 \pm 1.7$  kpc compared to  $18.2 \pm 2.4$  kpc). The 3CR galaxies at  $0.93 < z < 1.27$  are on average  $1.05 \pm 0.24$  mag more luminous in the  $R$ -band, and  $\sim 0.46$  dex larger, than our 6C galaxies at the same mean redshift (note that this result will not depend significantly on the assumed  $q_0$ ). This magnitude difference is greater than the 0.7 mag reported by Eales et al. (1997) for a  $z > 0.6$  sample, probably as a result of our exclusion of the less evolved 3CR galaxies at  $0.6 < z < 0.93$  and our use of total rather than metric magnitudes (giving a greater difference in luminosity between small and large galaxies).

To compare these galaxies with those at lower redshift, Figure 6 shows local  $r_{hl} - M_R$  relations, converted from the  $r_{hl} - M_B$  relations used by e.g. Roche et al. (1997) to the  $R$ -band assuming the  $z = 0$  colour of  $B - R = 1.44$  for ellipticals (as given by the model) and  $B - R = 1.0$  for spirals.

For ellipticals, the Bingelli, Sandage and Tarenghi (1984) relation becomes

$$\log(r_{hl}/\text{kpc}) = -0.3(M_R + 20.01)$$

for  $M_R < -21.44$ , and

$$\log(r_{hl}/\text{kpc}) = -0.1(M_R + 17.14)$$

for  $M_R > -21.44$ .

For spirals, the Freeman (1970) surface brightness becomes,

$$\log(r_{hl}/\text{kpc}) = -0.2M_R - 3.42$$

Figure 6 also shows an observed sample of low redshift radio galaxies, from Owen and Laing (1989), who estimated absolute magnitudes in the Cousins  $R$  band and bulge-model-fitted radii for  $z < 0.2$  radio galaxies of a number of types. We plot their Classical Double FR II (Fanaroff and Riley 1974) radio galaxies, the type most appropriate for comparison with the higher redshift samples, with sizes and magnitudes converted to  $H_0 = 50 \text{ km s}^{-1} \text{ Mpc}^{-1}$  and their isophotal absolute magnitudes extrapolated to total magnitudes assuming bulge profiles with their fitted effective and isophotal radii. These 24 low redshift ( $z_{mean} = 0.11$ ) radio galaxies are less luminous (mean  $M_R = -23.37 \pm 0.12$ ) than those at higher redshift, and have a very wide range of sizes with a mean  $r_{hl}$  of  $12.5 \pm 2.3$  kpc, intermediate between the 6C and 3CR galaxies.

The QSO is displaced far from the all other sources on this plot, on account of its central point-source. As we cannot measure the true galaxy size with this data, this object must be excluded from our discussion of  $r_{hl} - M_R$  relations.

The 6C galaxies are clearly shifted relative to the  $r_{hl} - M_R$  relation of local ellipticals, in the direction of a higher intrinsic SB. As noted by Best et al. (1997), the 3CR objects also tend to be enhanced in SB relative to local ellipticals. Note that estimates of the intrinsic SB will be independent of the assumed  $q_0$  and  $H_0$ . The  $r_{hl} - M_R$  relations of both the  $z \sim 0$  and  $z \sim 1$  radio galaxies do not appear to follow the  $\Delta(\log r_{hl}) = -0.2\Delta(M)$  slope of constant SB typical of spirals – they are noticeably steeper and more consistent with the  $\Delta(\log r_{hl}) = -0.3\Delta(M)$  slope of the giant ellipticals. Hence to estimate the surface brightness evolution  $\Delta R$  relative to local E/S0 galaxies of the same size, we fit the function

$$\log(r_{hl}/\text{kpc}) = -0.3(M_R + \Delta R + 20.01)$$

For the 7 6C galaxies we classed as bulge/generic types,  $\chi^2$  is minimized for  $\Delta R = 1.79 \pm 0.22$  mag, with a  $\chi^2$  of only 6.8 indicating that all 7 are consistent with this single  $r_{hl} - M_R$  relation. One of double objects (6C1011+36) lies on the same relation. It appears to be undergoing just a minor merger, of a large elliptical with a much less massive dwarf galaxy, and this might not greatly affect the total size or luminosity. However, the other double object (6C1256+36) and the ‘radio jet galaxy’ 6C1129+37 are of lower mean SB, corresponding to  $\Delta R = 1.01_{-0.13}^{+0.17}$  mag and  $\Delta R = 1.05_{-0.17}^{+0.07}$  mag respectively. The image of the 6C1256+36 galaxy was suggestive of an elliptical merging with a large, low surface brightness disk galaxy. This would obviously decrease the mean SB of the combined object and give it a more disk-like profile, while accounting for the central SB remaining high. In contrast, the radio jet object 6C1129+37 has a intrinsically low central SB as well as a low mean SB.

An error-weighted fit to all 10 6C objects gives  $\Delta R = 1.26 \pm 0.18$  mag, but with a high  $\chi^2$  of 62.16 indicating that the galaxies are not all consistent with a single  $r_{hl} - M_R$  relation – there is a significant difference between the two relatively low mean SB objects and the relation defined by the other 8. An unweighted fit of the same relation to the 24 low redshift FRII galaxies gives  $\Delta R = 0.12 \pm 0.19$  mag, consistent with unevolved ellipticals. An unweighted fit to the 21 3CR galaxies gives evolution of  $\Delta R = 0.80 \pm 0.15$  mag, rather less than for our sample. However, if we separately consider the lower redshift ( $0.47 < z < 0.92$ ) and higher redshift ( $0.92 < z < 1.27$ ) 3CR subsamples, the former gives  $\Delta R = 0.51 \pm 0.18$  and the latter  $\Delta R = 1.20 \pm 0.18$ . There appears to be surface brightness evolution of  $0.69 \pm 0.25$  mag between the respective mean redshifts of 0.73 and 1.10, with the higher redshift subsample being much closer in size-luminosity relation to the 6C galaxies at  $z_{mean} = 1.11$ . We discuss the implications in Section 7 below.

## 7. Discussion

### 7.1 Surface Brightness Evolution

Using ground-based data, we have carried out a preliminary investigation of the  $K$ -band angular size and morphology of 6C radio galaxies at  $1 < z < 1.4$ . Our first result is that the 6C galaxies typically have smaller  $K$ -band half-light radii than 3CR radio galaxies at similar redshifts. This appears to exclude the hypothesis that 3CR and 6C sources at  $z \sim 1$  have identical host galaxies and the higher  $K$ -band luminosity of the 3CR sources (e.g. Eales et al. 1997) is due solely to their more powerful active nuclei. If this was the case, the 3CR galaxies would have *smaller* half-light radii than their 6C counterparts, due to the greater dominance of the central point-sources. The difference in  $K$  luminosity appears to be due primarily to the stellar components, which in the 3CR galaxies are considerably larger and presumably more massive.

We estimate that the  $z_{mean} = 1.11$  6C galaxies show a mean surface brightness enhancement of  $1.26 \pm 0.18$  mag in the rest-frame Cousins  $R$ -band, relative to the  $r_{hl} - M_R$  relation of local ellipticals. This degree of evolution is consistent with the  $1.20 \pm 0.18$  mag we estimate for a subsample of more radioluminous 3CR galaxies at the same mean redshift. However, the 6C galaxies which most resembled normal ellipticals appeared to show greater SB evolution of  $1.79 \pm 0.22$  mag. One possible explanation for this higher estimate is that some radio galaxies contain central point sources, which with the limited resolution of our data are not distinguished from the underlying galaxy but do cause an underestimate of  $r_{hl}$ . This would cause the SB evolution to be overestimated, and if the effect on  $r_{hl}$  is very large might even account for the difference in the mean  $r_{hl}$  of the 3CR and 6C galaxies. To estimate the likely effect of point-source contamination, we consider a bulge-profile model with  $r_e = 1.8$  arcsec – the mean



size of the Best et al. (1997) 3CR galaxies – to which is added a central point-source contributing from 0% to 100% of the total flux. These models were convolved with seeing profiles and normalized to have  $K = 17.4$  with sky noise typical of the real Redeye data, and then analysed in the same way as the real radio galaxy images.

Figure 7 shows the estimated bulge-model  $r_e$  as a function of the point-source contribution to the total flux. A point-source component of 10% reduces the fitted  $r_e$  by  $\sim 25\%$ , so could increase the estimated  $\Delta R$  by 0.42 mag. This would be sufficient to account for much of the difference in the estimated  $|\Delta R|$  between the bulge/generic 6C galaxies and the 3CR galaxies. However, to reduce the fitted  $r_{hl}$  from 1.8 arcsec to 0.55 arcsec, the mean size of the 6C galaxies, would require a much larger point-source contribution of  $\geq 30\%$ . It is extremely unlikely that such luminous point-sources are typical of the 6C radio galaxies. Although we are at present only able to exclude a strong central point-source in the case of 6C1129+37 (for which we have WFPC2 data), only 2/21 of the 3CR galaxies of Best et al. (1997) had profiles consistent with any point-source component of  $\geq 10\%$  in the observed  $K$ -band, and if anything the less radioluminous 6C galaxies would be expected to show less nuclear activity.

Hence it seems that central point-sources would not make more than a small contribution to the difference in  $r_{hl}$  between 6C and 3CR galaxies, but they might still be present in the bulge/generic galaxies at the  $< 10\%$  level and be sufficient to cause an overestimate of the surface brightness evolution by up to  $\sim 0.42$  mag. This would still leave at least  $\sim 1.37$  mag of genuine evolution. This is still less than the surface brightness enhancement of  $z \sim 3$  galaxies on the Hubble Deep Field (e.g. Jones and Disney 1997; Roche et al. 1997b), so there is no doubt that such a degree of SB evolution is possible for large galaxies at  $z > 1$ .

In contrast, the SB of FR II radio galaxies at  $z_{mean} = 0.11$  showed only  $0.12 \pm 0.19$  mag of evolution relative to the local elliptical  $r_{hl} - M_R$  relation, so these objects are consistent with being unevolved ellipticals or with the 0.12 mag of passive evolution predicted by our model at their mean redshift. This confirms that the assumed  $r_{hl} - M_R$  relation is appropriate for powerful radio galaxies at low redshifts as well as for normal ellipticals, and hence that the  $r_{hl} - M_R$  relation of FR II radio galaxies in particular does shift with increasing redshift. As would be expected, a  $z_{mean} = 0.73$  subsample of 3CR galaxies showed intermediate evolution, estimated as  $0.51 \pm 0.18$  mag.

This progressive shift of the  $r_{hl} - M_R$  relation with increasing redshift is similar to that seen for normal radioquiet ellipticals over a similar redshift range. Schade et al. (1997) found the rest-frame blue-band surface brightness evolution of a mixture of field and cluster ellipticals to be best-fitted by  $0.78z$  mag for  $q_0 = 0.5$ , or  $\sim 0.92z$  mag for a low  $q_0$ . This is consistent with the passively evolving E/S0 model described in Section 6, which predicts  $\Delta(M_B) = -0.91$  mag at  $z = 1$ . In the rest-frame Cousins red-band, the model predicts slightly less evolution of  $\Delta(M_R) = -0.71$  mag, with 0.63 mag at  $z = 0.73$ , consistent with observations for the 3CR galaxies, and 0.75 mag at  $z = 1.11$ , a little less than observed. Hence there may be at least marginal indications that some  $z > 1$  radio galaxies in both the 3CR and 6C catalogs undergo more optical evolution than expected from passive evolution. This might be explained as the more rapid fading of those components of the radio galaxy luminosity not produced by old stellar populations, e.g. young stars formed along the radio jets (see Best et al. 1996), and diffuse scattered light from the central AGN. Note also that a steeper IMF could increase the rate of passive luminosity evolution.

## 7.2 Implications for Radio Galaxy Evolution

The simplest evolutionary scenario is that surface brightness changes but  $r_{hl}$  does not. Although there is probably some increase with time in the mean size of galaxies, angular sizes from WFPC2 data suggest that, for ellipticals, this is a small effect out to  $z \sim 1$  (e.g. Im et al. 1996; Roche et al. 1997). Assuming no evolution in  $r_{hl}$ , the estimated radii of the  $z \sim 1.1$  6C galaxies would on the basis of the assumed local  $r_{hl} - M_R$  relation indicate their local counterparts to have a mean absolute magnitude  $M_R = -22.6$ , i.e. about  $L^*$ , and therefore suggest that many evolve into  $L \sim L^*$  ellipticals. Most of the  $z < 0.2$  FR II radio galaxies in the Owen and Laing (1989) sample are ellipticals of modest size and  $L \sim L^*$  luminosity, although quite high radio luminosities of  $L(1400\text{MHz}) \simeq 10^{26.3} \text{ WHz}^{-1}$ . It is tempting to identify these as the low redshift counterparts of our 6C galaxies. Their typical radio luminosity corresponds to  $L(151\text{MHz}) \simeq 10^{27.2} \text{ WHz}^{-1}$  for the average SED of luminous radio galaxies ( $\alpha \simeq -0.94$ ), so this would require a factor of  $\sim 25$  decrease in radio luminosity since  $z \sim 1.1$ . This is consistent with the 6C radio luminosity function undergoing the same  $\tau = 3.3$  Gyr rate of evolution as estimated (Padovani and Urry 1992) for that of 3CR galaxies, but of course if our identification is correct

the evolution of the radio luminosity function must be due to the evolution of individual objects rather than simply a change in the number of galaxies which become powerful radio sources.

Owen and Laing (1989) and Owen and White (1991) found that the classical double FR II radio galaxies at  $z < 0.2$  were typically  $\sim 10^{1.6}$  higher in radio luminosity ( $L_{rad}$ ) than FRI galaxies of similar optical luminosity, with the dividing line between the classes following a  $L_{rad} \propto L_{opt}^2$  relation (Ledlow and Owen 1996). As previously reported by e.g. Longair and Seldner (1979) and Prestage and Peacock (1988, 1989), the FRI radio galaxies tended to lie within clusters (on average Abell class 0), while nearby FR IIs were usually in field environments. However, Yates, Miller and Peacock (1989) and Hill and Lilly (1991) found that powerful radio galaxies at higher redshifts ( $z \sim 0.5$ ) were as likely to lie in Abell class 0-1 clusters as in the field, suggesting a more rapid  $L_{rad}$  evolution for the sources in clusters.

If any of these 6C galaxies lie in rich clusters, their low redshift counterparts might instead be FRI galaxies, like the smaller of those in the Owen and White (1991) sample, with much lower present-day radio luminosities of  $L(1400\text{MHz}) \simeq 10^{24.7} \text{ WHz}^{-1}$ . This corresponds to  $L(151\text{MHz}) \simeq 10^{25.6} \text{ WHz}^{-1}$ , a factor of  $\sim 1000$  down on the  $L_{rad}$  of our 6C galaxies. Yee and Ellingson (1993) estimate that the optical luminosity evolution of AGN in rich cluster environments (Abell class  $\sim 1$ ) is as rapid as  $\tau \simeq 1.0 \pm 0.2$  Gyr out to  $z \sim 0.6$ , but at higher redshifts must be similar to other AGN. If this form of evolution is paralleled by the evolution of  $L_{rad}$  it would predict a decrease in  $L_{rad}$  of a factor of  $\sim 1000$  since  $z \sim 1.1$ , exactly the amount required.

We estimate that the mean  $M_R$  of 3CR and 6C galaxies at  $z \sim 1.1$  differs by  $1.05 \pm 0.24$  mag. The mean radius of the 3CR galaxies is much larger and with no size evolution would correspond to low-redshift counterparts with  $M_R = -24.2$ , several  $L^*$ . On this basis we suggest that the difference in 3CR and 6C luminosity at  $\lambda_{rest} \sim 1\mu\text{m}$  is due to a difference in the stellar masses of the host galaxies. As the radio luminosities differ by a factor  $\sim 6$ , this suggests a correlation  $L_{rad} \propto M_{stellar}^2$ .

A possible scenario explaining these observations is that;

(i) At  $z \geq 1$ , the maximum radio luminosity is strongly correlated with the stellar mass of the host galaxy, approximately as  $L_{rad} \propto M^2$ . This relation could physically be related to the higher pressure of surrounding gas, and perhaps the more massive central black hole, in a more massive galaxy (see e.g. Eales 1992; Rawlings and Saunders 1991). At  $z > 1$  many of the 3CR and 6C galaxies may be observed while close to this upper limit, with the 3CR galaxies typically being  $\sim 2.5$  times more massive and hence  $\sim 6$  times more radioluminous.

(ii) High redshift radio galaxies exist in a mixture of field and cluster environments. The peak  $L_{rad}$  attained during subsequent bursts of radio emission decreases more rapidly for radio galaxies in a rich cluster environment (Yee and Ellingson 1993). By  $z \sim 0$ , the cumulative effect of this environmental dependence amounts to a factor of  $\sim 10^{1.6}$  in  $L_{rad}$  between Abell class 0 environments and the field, obscuring the  $L_{rad} \propto M^2$  correlation seen at  $z \geq 1$ . However, as cluster environment also influences the evolution of the radio morphology, a  $L_{rad} \propto M^2$  correlation reappears when nearby radio galaxies are separated into FRI and FR II types (Ledlow and Owen 1996).

At any rate the high surface brightness and relatively small size of the 6C galaxies seems to argue that their evolution, at both optical and radio wavelengths, is no less rapid than that of the 3CR galaxies. Although the  $K - z$  relation of 6C galaxies may have appeared consistent with no evolution (Eales et al. 1997), their  $r_{hl} - M_R$  relation clearly is not. Of course, the results of this paper, being based on a small dataset of marginally adequate depth and resolution, can only be regarded as a preliminary. We intend to investigate larger numbers of  $z \sim 1$  radio galaxies, using NICMOS and ground-based adaptive optics to better constrain half-light radius and morphology, and to separate out bulge, disk, point-source and radio jet components.

## 8. Summary of Main Conclusions

(i) A sample of 6C radio galaxies at  $1 < z < 1.4$ , observed in the  $K$ -band, showed significant morphological diversity. Two appeared to be undergoing mergers, and another possessed two bright peaks aligned with the radio jets and may be closer to an exponential than a bulge profile, but the other seven were more consistent with normal elliptical morphologies in the  $K$ -band.

(ii) We estimated a mean half-light radius of  $6.1 \pm 1.3$  kpc for the 6C galaxies, which is similar to that of present-day  $L \sim L^*$  ellipticals and significantly smaller than the 3CR galaxies studied by Best et al. (1997). The difference between the measured sizes of 6C and 3CR galaxies cannot be accounted for

by point-source contamination, unless at the  $\geq 30\%$  level, which seems implausible on the basis of the lack of point-sources in the 3CR galaxies. Hence the difference in  $\lambda_{rest} \sim 1\mu\text{m}$  luminosity between 3CR and 6C galaxies at  $z \sim 1.1$  must result from a difference in the sizes of the host galaxies, and not solely from a difference in the power of the central nuclei.

(iii) The size-luminosity relation of the 6C galaxies at  $z \sim 1.1$  is offset from that of either local ellipticals or FRII radiogalaxies at  $z < 0.2$ , indicating 1.0–1.8 magnitudes of surface brightness evolution in the rest-frame  $R$ -band. This is similar to the 1.20 mag of surface brightness evolution seen for 3CR galaxies at the same redshift, suggesting that the 6C galaxies are undergoing a similar amount of evolution at optical wavelengths.

(iv) The sizes of the 6C galaxies are consistent with their low-redshift counterparts being FRII radio galaxies like those studied by Owen and Laing (1989), a factor of  $\sim 25$  lower in radio luminosity, suggesting radio luminosity evolution similar to the Padovani and Urry (1992) estimate for 3CR galaxies. Any 6C galaxies which lie in clusters may undergo a much greater reduction in radio luminosity to become FRI objects.

## Acknowledgements

Nathan Roche acknowledges the support of a PPARC research associateship, and some useful discussions with Kavan Ratnatunga on the analysis of faint galaxy images. We thank Garrett Cotter for help with the observations.

## References

- Allington-Smith, J.R., 1982. *Mon. Not. R. astr. Soc.*, **199**, 611.
- Allington-Smith, J.R., Perryman, M., Longair, M.S., Gunn, J.E. and Westphal, J.A., 1982. *Mon. Not. R. astr. Soc.*, **201**, 331.
- Best, P.N., Longair, M.S. and Röttgering, H., 1996. *Mon. Not. R. astr. Soc.*, **280**, L9.
- Best, P.N., Longair, M.S. and Röttgering, H., 1997. Preprint.
- Binggeli, B., Sandage, A. and Tarenghi, M. 1984. *Astron. J.*, **89**, 64.
- Bruzual, G. and Charlot, S., 1993. *Astrophys. J.*, **405**, 538.
- Dunlop, J.S. and Peacock, J.S., 1993. *Mon. Not. R. astr. Soc.*, **263**, 936.
- Eales, S., 1982. *Astrophys. J.*, **397**, 49.
- Eales, S., 1985. *Mon. Not. R. astr. Soc.*, **217**, 149.
- Eales, S. and Rawlings, S., 1996. *Astrophys. J.*, **367**, 1.
- Eales, S., Rawlings, S., Law-Green, D., Cotter, G. and Lacy, M., 1997. *Mon. Not. R. astr. Soc.*, in press.
- Fanaroff, B.L. and Riley, J.M., 1974. *Mon. Not. R. astr. Soc.*, **167**, 31p.
- Freeman, K., 1970. *Astrophys. J.*, **160**, 811.
- Hill, G.J. and Lilly, S.J., 1991. *Astrophys. J.*, **367**, 1.
- Im, M., Griffiths, R.E., Ratnatunga, K.U., and Sarajedini, V.L., 1996. *Astrophys. J.*, **461**, L79.
- Jones, B. and Disney, M., 1996. *HST and the High Redshift Universe*, eds. N.R. Tanvir, A. Aragón-Salamanca and J.V. Wall, 37th Herstmonceux Conference, Cambridge.
- Laing, R.A., Riley, J.M. and Longair, M.S., 1983. *Mon. Not. R. astr. Soc.*, **204**, 151.
- Ledlow, M. and Owen, F.N., 1996. *Astron J.*, **112**, 9.
- Leyshon, G. and Eales, S., 1997. *Mon. Not. R. astr. Soc.*, submitted.
- Lilly, S.J. and Longair, M.S., 1984. *Mon. Not. R. astr. Soc.*, **211**, 833.
- Lilly, S.J., MacLean I.S. and Longair, M.S., 1984. *Mon. Not. R. astr. Soc.*, **209**, 401.
- Longair, M.S. and Seldner, M., 1979. *Mon. Not. R. astr. Soc.*, **189**, 433.
- Owen, F.N. and Laing, R.A., 1989. *Mon. Not. R. astr. Soc.*, **238**, 357.
- Owen, F.N. and White, R.A., 1991. *Mon. Not. R. astr. Soc.*, **249**, 164.
- Padovani, P. and Urry, C.M., 1992. *Astrophys. J.*, **387**, 449.

- Prestage, R. and Peacock, J.A., 1988. *Mon. Not. R. astr. Soc.*, **230**, 131.
- Prestage, R. and Peacock, J.A., 1989. *Mon. Not. R. astr. Soc.*, **236**, 959.
- Rawlings, S., et al., 1997. In preparation.
- Rawlings, S. and Saunders, R., 1991. *Nature*, **349**, 138.
- Ridgway, S.E. and Stockton, A., 1997. *Astron. J.*, in press.
- Rigler, M.A., Lilly, S.J., Stockton, A., Hammer, F., LeFevre, O.N., 1992. *Astrophys. J.*, **385**, 61.
- Rigler, M.A. and Lilly, S.J., 1994. *Astrophys. J.*, **427**, L79.
- Roche, N., Ratnatunga, K., Griffiths, R.E., and Im, M., 1997. *Mon. Not. R. astr. Soc.*, submitted.
- Schade, D., Barrientos, L. and López-Cruz, O., 1997. *Astrophys. J.*, **477**, L17.
- Tadhunter, C.N., Scarrott, S.M., Draper, P. and Rolph, C., 1992. *Mon. Not. R. astr. Soc.*, **256**, 53P.
- Wainscoat, R.J., and Cowie, L., 1992. *Astron. J.*, **103**, 323.
- Yates, M.G., Miller, L. and Peacock, J.A., 1989. *Mon. Not. R. astr. Soc.*, **240**, 129.
- Yee, H.K.C. and Ellingson, E., 1993. *Astrophys. J.*, **411**, 43.

## Table Captions

**Table 1.** The co-ordinates of the 11 radio galaxies, their  $K$ -band magnitudes as measured from this data, their spectroscopic redshifts, and the detection thresholds of the Redeye images.

**Table 2.** A comparison of the areas of each radio galaxy above a series of 8 thresholds with those given by model profiles; (i) the  $\chi^2$  for a point-source model; (ii) the  $\chi^2$  and exponential scalelength (with  $\pm 1\sigma$  errors) of the best-fitting disk-profile model; (iii) the  $\chi^2$  and effective radius (with  $\pm 1\sigma$  errors) of the best-fitting bulge-profile model.

**Table 3.** Estimated absolute magnitude in the rest-frame  $K$ -band, the ellipticity of the radiogalaxy images as determined by PISA, and the half-light radius of the best-fitting model (with  $\pm 1\sigma$  errors), corrected for inclination.

## Figure Captions

**Figure 1.** Grey-scale plots of  $15 \times 15$  arcsec areas of the  $K'$ -band Redeye images centred on each radio galaxy. North is at the top, east at the left. Top row (left to right): 6C0822+39, 6C0943+39, 6C1011+36. Second row: 6C1017+37, 6C1123+34, 6C1129+37. Third row: 6C1204+35, 6C1217+36, 6C1256+36. Bottom row, 6C1257+36, 5C6.8.

**Figure 2.** Contour plots of the images on Figure 1.

**Figure 3.** Histograms of the area (in  $0.5 \times 0.5$  arcsec pixels) of each radio galaxy image above a series of 8 intensity thresholds defined by PISA (the lowest being the detection threshold given in Table 1). The plots also show the areas measured above the same thresholds for a point-source (long-dashed) model, the best-fitting disk model (dotted), and the best-fitting bulge model (short dash), when convolved with the seeing profile and normalized to the same total intensity as the galaxies.

**Figure 4.** Radial intensity profiles of the radio galaxies on the Redeye images, shown as the mean surface brightness in  $K$  mag arcsec $^{-2}$  (with  $\pm 1\sigma$  errors) in annuli of 0.5 arcsec width around the image centroid, together with a point-source (long-dashed) model, the best-fitting disk model (dotted), and the best-fitting bulge model (short dash), all convolved with the seeing profile and normalized to the same total intensity as the galaxies.

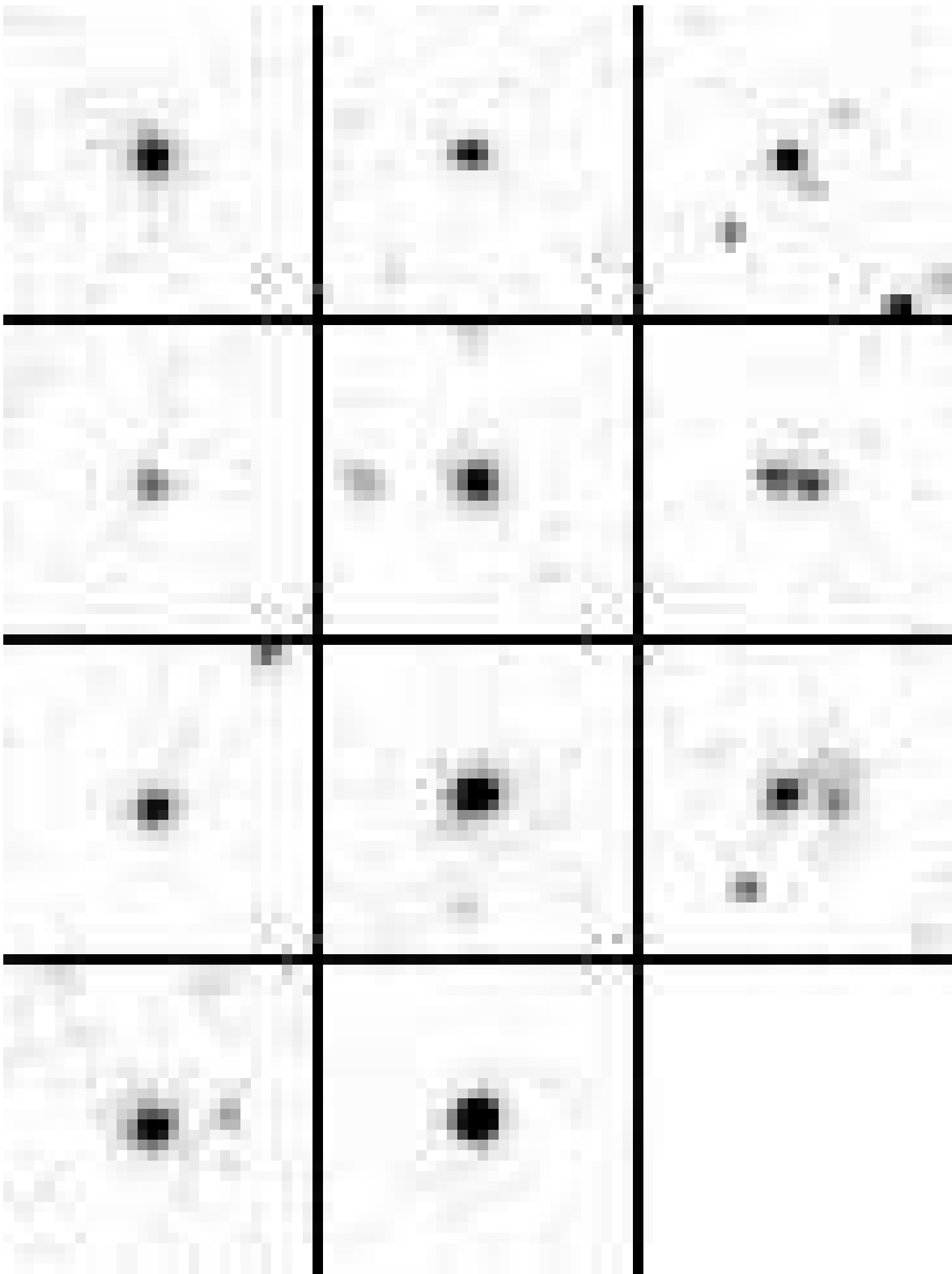
**Figure 5.** Modelled magnitude correction between the observer-frame  $K$ -band and rest-frame Cousins  $R$ -band, as a function of redshift, for a passively evolving E/S0 galaxy model and a model with a constant star-formation rate.

**Figure 6.** Estimated half-light radius (in kpc) against rest-frame  $R$ -band absolute magnitude for the 6C radio galaxies, with symbols indicating morphology, together with the 3CR radio galaxies from Best et

al. (1997), the low-redshift FR II galaxies from Owen and Laing (1989), and assumed  $r_{hl} - M_R$  relations for local ellipticals (dashed line) and spirals (dotted line).

**Figure 7.** Bulge-model half-light radius ( $r_e$ ) measured as described in Section 4 for a simulated  $r_e = 1.8$  arcsec bulge-profile galaxy to which is added an increasingly luminous central point-source.

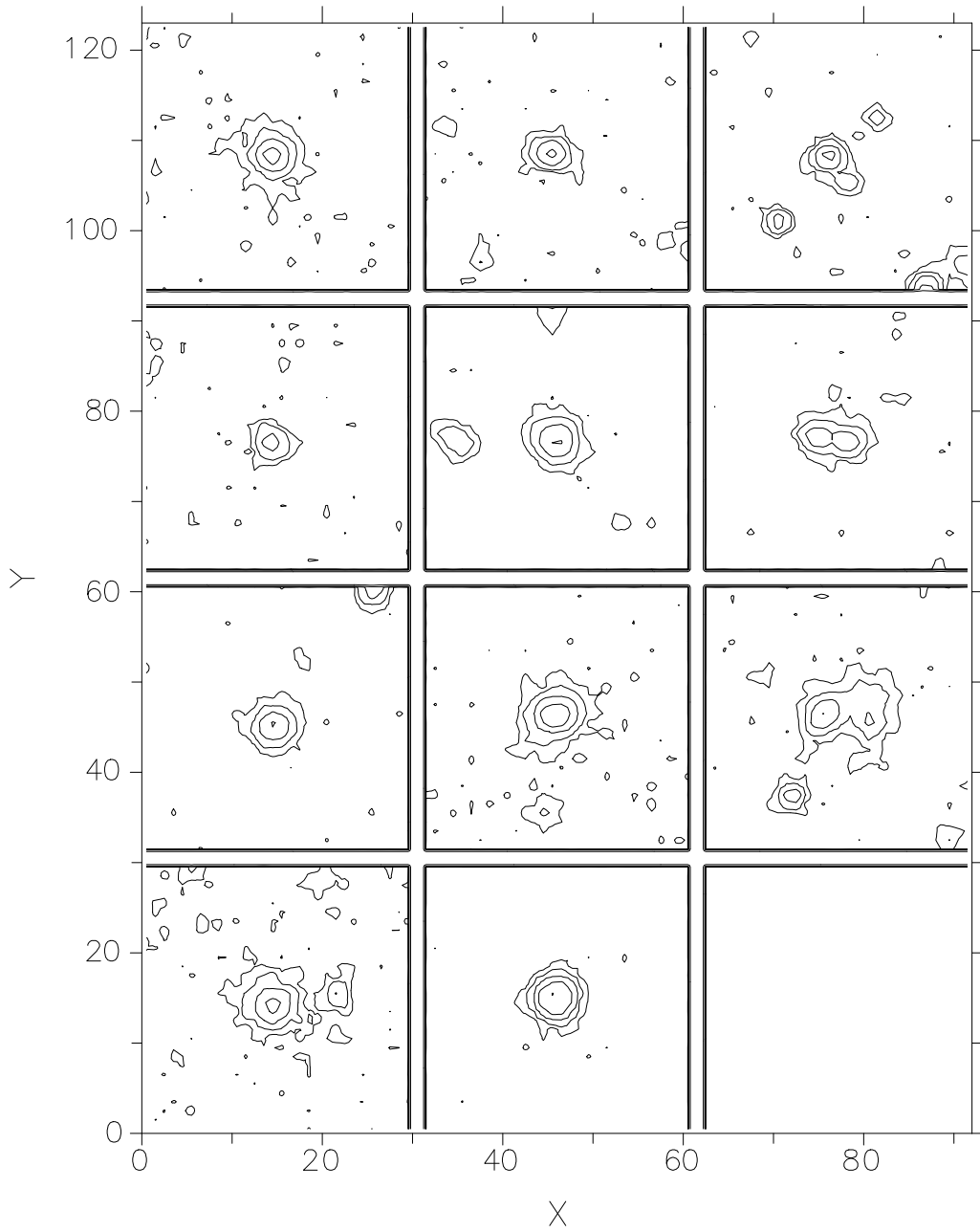






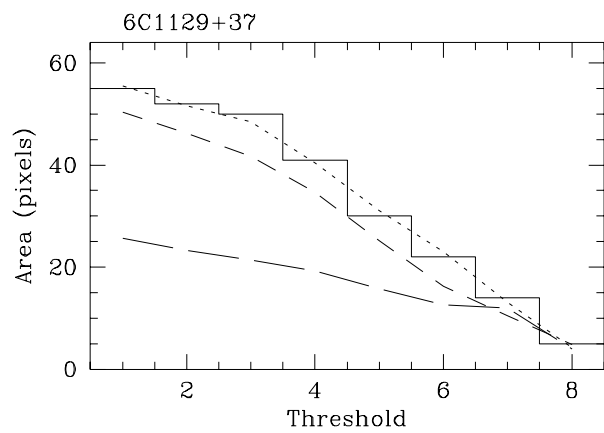
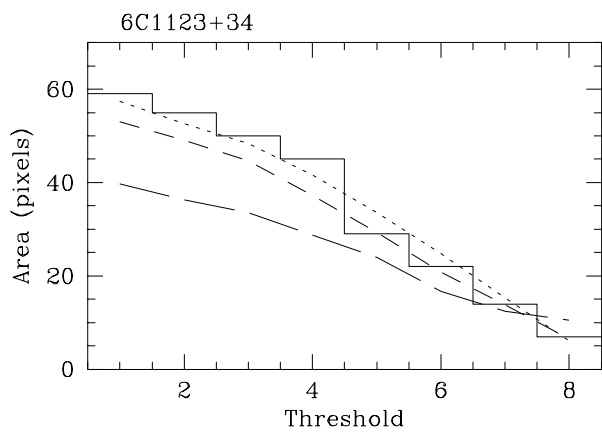
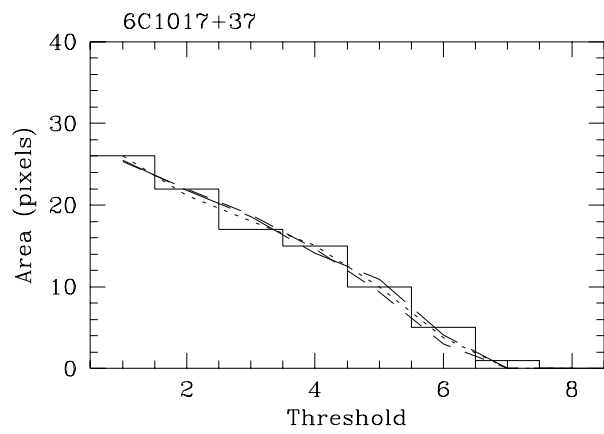
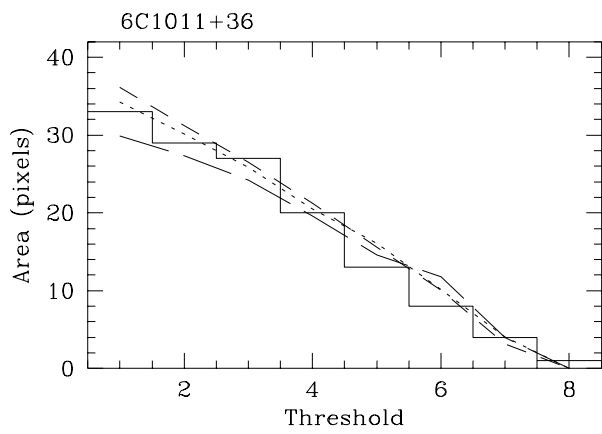
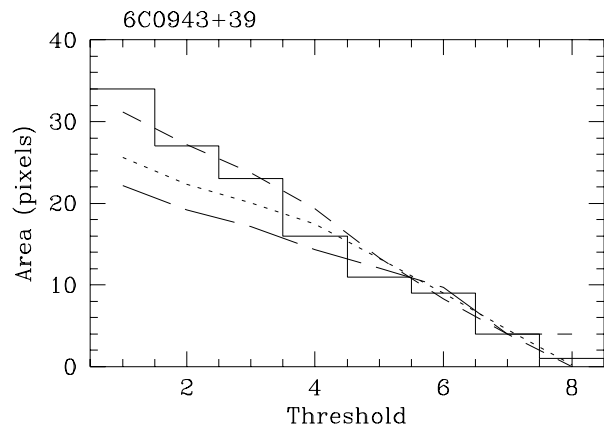
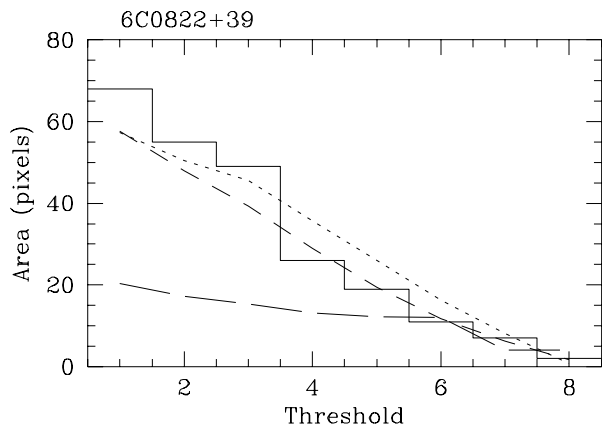


# KAPPA - Quilt

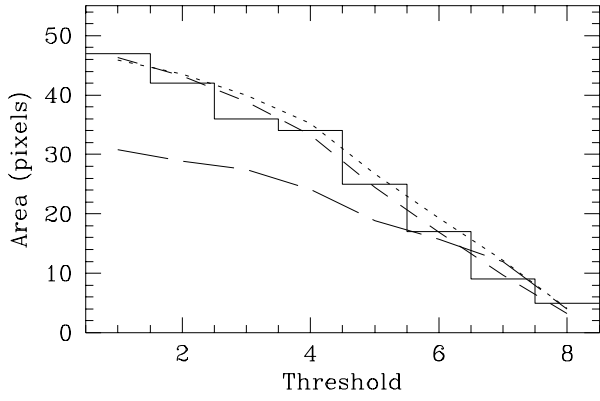


Contour heights

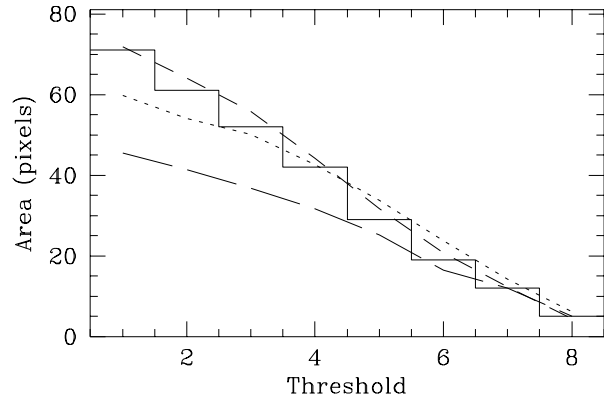
- 1 : 62.79716
- 2 : 157.7393
- 3 : 396.2233
- 4 : 995.2679
- 5 : 2500



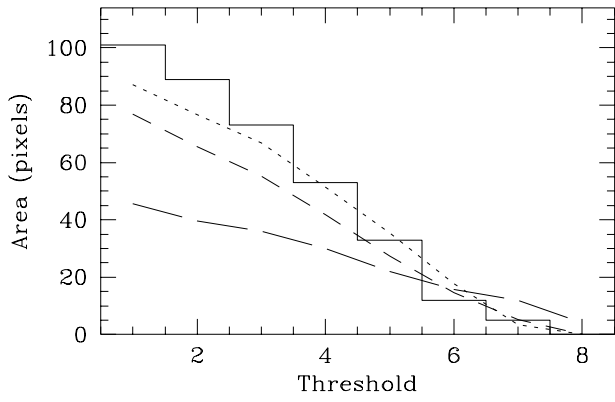
6C1204+35



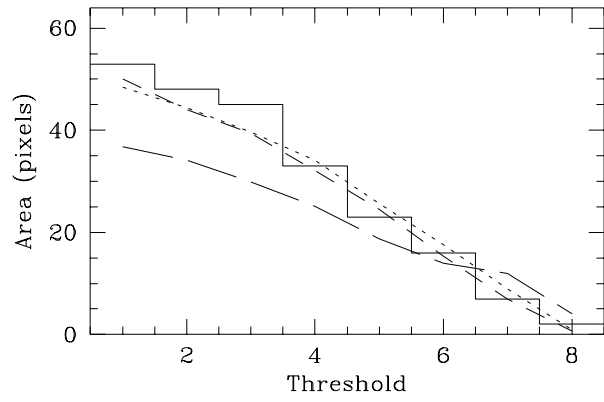
6C1217+36



6C1256+36



6C1257+36



5C6.8

